

MAGNet: Motif-Agnostic Generation of Molecules from Shapes

Leon Hetzel^{*1,2,3} Johanna Sommer^{*1,3} Bastian Rieck^{1,2} Fabian Theis^{1,2,3}
Stephan Günnemann^{1,3}

¹School of Computation, Information, and Technology, Technical University of Munich

²Helmholtz Munich

³Munich Data Science Institute, Technical University of Munich

Abstract

Recent advances in machine learning for molecules exhibit great potential for facilitating drug discovery from *in silico* predictions. Most models for molecule generation rely on the decomposition of molecules into frequently occurring substructures (motifs), from which they generate novel compounds. While motif representations greatly aid in learning molecular distributions, such methods struggle to represent substructures beyond their known motif set. To alleviate this issue and increase flexibility across datasets, we propose MAGNet, a graph-based model that generates abstract shapes before allocating atom and bond types. To this end, we introduce a novel factorisation of the molecules' data distribution that accounts for the molecules' global context and facilitates learning adequate assignments of atoms and bonds onto shapes. While the abstraction to shapes introduces greater complexity for distribution learning, we show the competitive performance of MAGNet on standard benchmarks. Importantly, we demonstrate that MAGNet's improved expressivity leads to molecules with more topologically distinct structures and, at the same time, diverse atom and bond assignments.

1 Introduction

The generation of de novo compounds through machine learning models has become increasingly important in various fields, such as drug discovery, material science, and chemistry (Bian and Xie 2021; Butler et al. 2018; Choudhary et al. 2022; Hetzel et al. 2022; Moret et al. 2023). These models promise a more efficient exploration of the vast chemical space and generation of novel compounds with specific properties by leveraging their learned representations, potentially leading to the discovery of molecules with unique properties that would otherwise go undiscovered (Zhou et al. 2019; Hoffman et al. 2022).

Following Du et al. (2022), generative models for molecules can be categorised into (i) combinatorial optimisation methods, which operate on the molecular graph directly, and (ii) deep generative models, which map molecules to a continuous latent space. For deep generative models,

* These authors contributed equally.

the ability to express discrete molecules through latent representations depends heavily on the semantic meaning encoded in the latent space. Although much of the literature emphasises the sequential, step-by-step, decoding approach for molecules (Yu and Gao 2022; Yang et al. 2022), the influence of a molecule’s latent representation on the decoding process and its interplay with the partially generated molecule remain unclear. In the worst-case scenario, the latent representation has an impact only on the initial decoding step, while subsequent generation steps become more and more independent. In contrast, all-at-once methods fully rely on the latent space representation, as there are no partially generated molecules to extend.

Often, vocabularies of motifs, frequently occurring subgraphs, are used to obtain meaningful representations. Such vocabularies are augmented by individual atoms, aiming to effectively capture the underlying distribution while preserving the ability to represent diverse molecular structures (Sommer et al. 2023). However, our findings demonstrate that this promise remains unfulfilled. Models that rely on a combination of motifs and single atoms struggle to reliably construct uncommon structures solely from individual atoms. This has significant implications: the tail regions of the molecular distribution are not effectively learned, resulting in the inability to sample rare structures and potential downstream tasks being performed on the “mean set” of the distribution.

Upon quantification, the significance of the distribution tail becomes evident. Out of the 7987 subgraphs in ZINC, models proposed by Maziarz et al. (2022) and Kong et al. (2022) include less than 10% of subgraphs in their motif vocabulary. A naive solution would be to increase the vocabulary size. However, taking into account that the chemical space is estimated to have a size of 10^{60} , it becomes evident that motif-based approaches lack the ability to represent molecular distributions in its entirety.

In this work, we propose a more principled way to navigate the chemical space and learn molecular distributions accurately: MAGNet. Instead of relying on a motif vocabulary, we abstract subgraphs to shapes and enable our model to learn adequate atom and bond allocations to a given shape, cf. Fig. 1. We circumvent a combinatorial explosion of the vocabulary—a challenge that motif-based approaches face—by disentangling structure and features of molecules. The abstraction to shapes requires an understanding of a molecule at a global level, as multiple subgraphs may share the same underlying shape. In the decoding process, MAGNet constructs a shape hypergraph directly from the latent representation of a molecule, representing the multiset of shapes and their interconnections. This holistic perspective enables atom and bond allocations to the respective shapes that are diverse and match the underlying molecular distribution.

The contributions of this work are as follows:

- A novel factorisation approach for the distribution of molecular graphs, effectively disentangling the structure from feature prediction, enabling more flexible representations
- MAGNet, an all-at-once approach for molecule generation which incorporates the global context of a molecule throughout the entire generation process

2 The MAGNet model

To enable generating the great variety of different molecular structures, we propose to further abstract motifs to shapes. This leads to a much smaller space and, thus, more tractable learning of

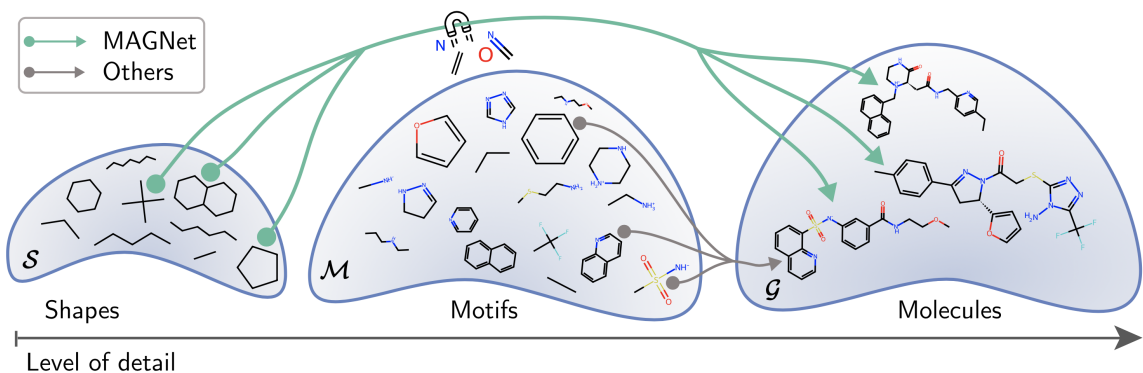


Figure 1: Current methods use motifs to compose new molecules. MAGNet goes one step further and abstracts molecular subgraphs to untyped shapes. Agnostic to atom and bond features in the beginning of the generation process, MAGNet generates molecules with great structural variety.

the underlying shape distribution, see Fig. 1. Since motif vocabularies are limited in size, such a shape abstraction improves expressivity with respect to the graph structures that can be learned and sampled. Yet, it also introduces the challenge of learning the shape representation, i.e. the map from a shape without node or edge features to a chemically valid subgraph with atoms and bonds: the same shape can occur in different molecular contexts which requires providing more information than the local shape structure before identifying atom and bond types. Subsequently, we first describe how we factorise the data distribution to provide sufficient context and then describe the MAGNet model.

2.1 Factorising the data distribution $\mathbb{P}(\mathcal{G})$

A molecular graph \mathcal{G} is defined by its structure together with its node and edge features, describing atoms and bonds, respectively. In this work, we consider a factorisation of $\mathbb{P}(\mathcal{G})$ that splits the molecular graph \mathcal{G} into its core structure \mathcal{C} and its leaves \mathcal{L} :

$$\mathbb{P}(\mathcal{G}) = \mathbb{P}(\mathcal{L} \mid \mathcal{C}) \mathbb{P}(\mathcal{C}),$$

where the set of leaves \mathcal{L} contains all atoms i with degree $d_i = 1$ and whose neighbour atom j has a degree $d_j > 2$, i.e. $i \in \mathcal{L}$ is not the end-point of a chain. Formally, $\mathcal{L} := \{i \mid d_i = 1 \wedge d_j > 2 \forall j \in \mathcal{N}_i\}$, where \mathcal{N}_i refers to the neighbourhood of node i . We call the remaining graph the core molecule $\mathcal{C} := \mathcal{G} \setminus \mathcal{L}$ and provide an illustrative example in Fig. 2.

To factorise $\mathbb{P}(\mathcal{C})$ further, we first consider a fragmentation of the core’s structure into a multiset of shapes \mathcal{S} and the typed connectivity $A \in \{0, \text{C}, \text{N}, \dots\}^{|\mathcal{S}| \times |\mathcal{S}|}$ between shapes $S \in \mathcal{S}$. Each shape $S \in \mathcal{S}$ can be classified as one of three categories, namely (i) rings, (ii) junctions, and (iii) chains. A shape S only holds *structural information* about its $s = |S|$ nodes, meaning we can represent it as a matrix, i.e. $S \in \{0, 1\}^{s \times s}$. The shape connectivity A , on the other hand, is typed and encodes whether two shapes share a node, signified by $A \neq 0$, and also the respective atom type of the join, e.g. C or N. Note that since \mathcal{S} and A are shape-level representations, the exact position of the join within shapes remains undefined at this stage; see Fig. 2. Since all cyclic structures within the

molecular graph are considered individual shapes, A always describes a tree on the shape-level. Further, if a shape S is equipped with node and edges features, i.e. atom and bond types, we consider this representation of S to constitute a typed subgraph M of the input graph, and the associated multiset within the molecule \mathcal{M} . We note that a shape S can map to different ‘ M ’s as only the binary adjacencies will be shared between them; we will later on make use of context knowledge to select a suitable M . The shape representations \mathcal{M} and the shape connectivity A do not fully describe \mathcal{C} yet as information about the explicit join positions is missing. For this, we use the join set \mathcal{J} which can be understood as the set of join nodes j that are contained in two motifs: $\mathcal{J} = \{j \mid j \in M_k, j \in M_l, A_{kl} \neq 0, S_k, S_l \in \mathcal{S}\}$. Taken together, we can express $\mathbb{P}(\mathcal{C})$ as:

$$\begin{aligned}\mathbb{P}(\mathcal{C}) &= \mathbb{P}(\mathcal{M}, \mathcal{J}, \mathcal{S}, A) \\ &= \mathbb{P}(\mathcal{J} \mid \mathcal{M}, A) \mathbb{P}(\mathcal{M}, \mathcal{S}, A) \\ &= \mathbb{P}(\mathcal{J} \mid \mathcal{M}, A) \mathbb{P}(\mathcal{M} \mid \mathcal{S}, A) \mathbb{P}(A \mid \mathcal{S}) \mathbb{P}(\mathcal{S}),\end{aligned}$$

where we have used that \mathcal{J} is *conditionally independent* of \mathcal{S} given the motifs \mathcal{M} and factorised $\mathbb{P}(\mathcal{C})$ in a hierarchical fashion.

During learning, we start with the coarser shape-level, that is \mathcal{S} and A , and then proceed to the atom level for \mathcal{M} and \mathcal{J} . Finally, we learn the distribution of leaves \mathcal{L} conditioned on the constructed core molecule \mathcal{C} . Note that unlike autoregressive methods, this factorisation considers the complete molecule at all times with only the level of detail increasing at each step.

A matching fragmentation scheme for molecule decomposition Our factorisation requires a fragmentation scheme that separates the leaves \mathcal{L} from the core \mathcal{C} of a molecule and identifies the shape representations \mathcal{M} as well as joins \mathcal{J} . Knowing \mathcal{M} and \mathcal{J} , \mathcal{S} and A readily follow. To this end, we first identify all leaf atoms and, subsequently, decompose the core into cyclic and non-cyclic subgraphs (Jin, Barzilay, and Jaakkola 2020; Maziarz et al. 2022). Between the latter, we further distinguish between junctions and chains. This kind of molecule decomposition can readily be achieved by some adjustments to the breaking bridge bonds fragmentation and is described in detail in Appendix A. Applying our fragmentation to ZINC (Irwin et al. 2020), we cover the complete dataset with only 540 shapes in total.

2.2 The MAGNet decoder

MAGNet represents a VAE model (Kingma, Salimans, and Welling 2015), where the latent vectors z are trained to encode meaningful semantics about the input data. We choose an architecture that closely follows the hierarchy from Section 2.1, cf. Fig. 2. That is, given a vector z from the latent space, MAGNet’s generation process first works on the shape level to predict the shape multiset \mathcal{S} and the connectivity A between shapes before going to the atom level for the motif and join representations, \mathcal{M} and \mathcal{J} , respectively.

Shape multiset \mathcal{S} Our model starts with decoding the shape multiset—the same shape can occur multiple times in one molecule—from the latent representation z . More specifically, we represent $\mathbb{P}(\mathcal{S} | z)$ conditioned on the already sampled shapes:

$$\mathbb{P}(\mathcal{S} | z) = \prod_{i=1}^n \mathbb{P}(S_i | \bigcup_{j<i} S_j, z),$$

which we realise by an RNN module and optimise using a Cross-Entropy (CE) loss with shapes being ordered according to the canonical atom rank (Weininger et al. 1989).

Shape connectivity A Given the shape multiset \mathcal{S} , MAGNet infers the connectivity A between shapes $S_i, S_j \in \mathcal{S}$. Formally, we learn

$$\mathbb{P}(A | \mathcal{S}, z) = \prod_{i,j=1}^n \mathbb{P}(A_{ij} = t | \mathcal{S}, z),$$

where $t \in \{0, C, N, \dots\}$ not only encodes the existence (or absence) of a shape connection but also its atom type. Further, we assume the individual connections A_{ij} and A_{lk} to be independent given the shape multiset \mathcal{S} and the latent representation z . MAGNet realises this connectivity module through an MLP, optimised with CE loss.

Atom and Bond allocations \mathcal{M} The shape set \mathcal{S} and connectivity A fully describe MAGNet’s shape-level representation. To proceed to the atom level, node and edge features have to be assigned per shape, which can be expressed according to:

$$\mathbb{P}(M_i | \mathcal{S}, A, z) = \prod_{p_a \in V_{S_i}} \mathbb{P}(p_a = a | \mathcal{S}, A, z) \prod_{p_b \in E_{S_i}} \mathbb{P}(p_b = b | \mathcal{S}, A, z),$$

where p_a and p_b refer to the canonical positions of nodes V_{S_i} and edges E_{S_i} in the shape, respectively, and M_i to the shape representation of the considered shape S_i including atoms a and bonds b . MAGNet realises $\mathbb{P}(M_i | \mathcal{S}, A, z)$ through a RNN module that sequentially goes through all positions p_k , i.e.

$$\mathbb{P}(M_i^k | \mathcal{S}, A, z) = \prod_{p_i^k} \mathbb{P}(p_i^k = k_i | \mathcal{S}, A, \bigcup_{j<i} p_j^k, z),$$

where k refers to atoms a or bonds b ($k = a, b$). Note that conditioning on A ensures that M_i includes all atoms required for connectivity also on the atom-level, i.e. the atom allocations for M have to respect all join types defined by the shape connectivity A : $\bigcup_j A_{ij} \subseteq \bigcup_j M_i^a \cap M_j^a$.

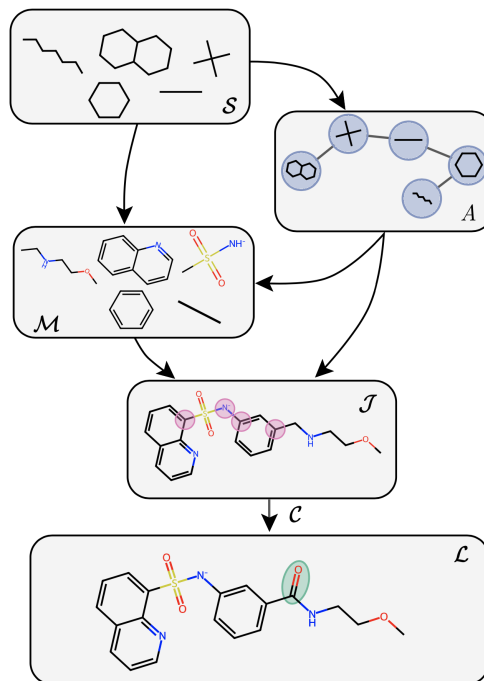


Figure 2: MAGNet’s decoding flow. Starting from the shape multiset \mathcal{S} , the shape connectivity A is predicted. A and \mathcal{S} together map to the shape representations \mathcal{M} which are joined on the atom level as defined by the join set \mathcal{J} . The resulting core molecule \mathcal{C} is then extended with leaves \mathcal{L} to complete the molecule \mathcal{G} .

Join nodes \mathcal{J} Finally, to fully define the core molecule \mathcal{C} , one has to identify the specific atom positions p_a that have to be merged and are included in the join set \mathcal{J} , i.e.

$$\mathbb{P}(\mathcal{J} \mid \mathcal{M}, A, z) = \prod_{\substack{k,l \\ k \neq l}} \prod_{\substack{i \in M_k, \\ j \in M_l}} \mathbb{P}(p_i \equiv p_j \mid \mathcal{M}, A, z) = \prod_{\substack{k,l \\ k \neq l}} \prod_{\substack{i \in M_k, \\ j \in M_l}} J_{ij}^{(k,l)},$$

where the RHS expresses the merge probability of nodes i and j in shape representations M_k and M_l , respectively. Within MAGNet, the join matrix $J^{(k,l)} \in [0, 1]^{V_{S_k} \times V_{S_l}}$ is learned through a MLP and optimised via binary CE. Crucially, joins, i.e. $J_{ij}^{(k,l)} \neq 0$, are only allowed between identical atom types p_i and p_j that match A_{kl} . The identification of the join set \mathcal{J} completes the core molecule.

Leaves \mathcal{L} Predicting $\mathbb{P}(\mathcal{L} \mid \mathcal{C})$ means two things: identifying the correct atom type of the leaf L and also its attachment to the core molecule \mathcal{C} . Similar to $\mathbb{P}(M_i \mid \mathcal{S}, A, z)$, we factorise the distribution with respect to the shape set, i.e.

$$\mathbb{P}(\mathcal{L} \mid \mathcal{C}, z) = \prod_{S \in \mathcal{S}} \mathbb{P}(\mathcal{L}_S \mid \mathcal{C}, z),$$

where \mathcal{L}_S refer to all leaves attached to all nodes $i \in S$. To learn $\mathbb{P}(\mathcal{L}_S \mid \mathcal{C}, z)$ we go through each node position in the shape representation:

$$\mathbb{P}(\mathcal{L}_S \mid \mathcal{C}, z) = \prod_{p_i \in S} \mathbb{P}(L_i \mid \mathcal{C}, \bigcup_{j < i} L_j, z),$$

which is realised by an RNN module. Different to before, we are now able to condition on the whole core molecule \mathcal{C} where the specific representation is achieved by a forward pass through MAGNet’s encoder (see Section 2.3) together with the respective shape representation M .

2.3 The MAGNet encoder

MAGNet’s encoder aims to learn the approximate posterior $Q(z \mid \mathcal{G})$. At its core, the encoder builds on the graph transformer by Shi et al. (2021) to create initial node embeddings of the molecular graph. To match the graph encoding with the individual modules described in Section 2.2, we include MLPs to aggregate the different classes of nodes and compute latent variables of shapes z_S , joins $z_{\mathcal{J}}$, and leaves $z_{\mathcal{L}}$. In regards to A , the shape aggregations are additionally processed in a GNN to obtain z_A . Since these representations have a dependency structure, we include a MLP to map to MAGNet’s latent space and observe the final graph embedding z . More details about the specific node features that are used and the dimensions of the encoder can be found in Appendix C.

Taken together, we optimise MAGNet according to the normal VAE setting, maximising the ELBO:

$$\begin{aligned} L &= \mathbb{E}_{z \sim Q} [\mathbb{P}(\mathcal{G} \mid z)] + \beta D_{\text{KL}}(Q(z \mid \mathcal{G}) \mid P) \quad \text{with } P \sim \mathcal{N}(0, \mathbb{1}) \\ &= L_S + L_A + L_M + L_{\mathcal{J}} + L_{\mathcal{L}} + \beta D_{\text{KL}}, \end{aligned}$$

where the KL-divergence D_{KL} enforces a Normal distribution P in the latent space, weighted by β .

3 Experiments

We organise our experiments in three sections. In the first part, Section 3.1, we establish MAGNet’s overall competitive performance on standard benchmarks. Moreover, we show that MAGNet is able to sample uncommon structures by leveraging its shape abstractions while also identifying meaningful atom and bond allocations. We complement this analysis by querying the learned latent space and interpolate between molecules. Building on these results, we continue to analyse the representative power of MAGNet in Section 3.2. Our experiments point towards a fundamental flaw present in motif-based approaches, indicating that shape abstractions are required if trained models are meant to be deployed in various drug discovery applications beyond the ZINC data. To further support this hypothesis, we investigate the zero-shot generalisation capabilities of the considered models in Section 3.3.

Baselines We consider five state-of-the-art molecule generation models as baselines. As a representative for an all-at-once approach (AAO), we consider PS-VAE (Kong et al. 2022), a two-step VAE that first decodes the multiset of a molecule’s motifs and atoms and then predicts their connection. Unlike PS-VAE, all other baselines are autoregressive in nature. Maziarz et al. (2022) propose MoLeR, a model that sequentially decodes a molecule by predicting the next atom or motif, then choosing its attachment point and, finally, the attachment bond type. Both methods rely on a motif vocabulary (Sommer et al. 2023) whose size is set to 512 for all experiments. Additionally, we include JTVAE, an autoregressive model that guides its molecule generation by building up a junction tree where nodes represent fragments (Jin, Barzilay, and Jaakkola 2018). Similar to MAGNet, HierVAE builds a multi-resolution representation and decodes a molecule in a fine-to-coarse manner (Jin, Barzilay, and Jaakkola 2020). For model training and inference, we rely on the optimal hyperparameters as specified by the authors. Details on MAGNet’s hyperparameters, training, and hardware are discussed in more detail in Appendix B.

Data We conduct experiments on the ZINC dataset (Irwin et al. 2020) which consists of 249,456 compounds. We use the dataset split specified by specified in Kusner, Paige, and Hernández-Lobato (2017). In addition, we employ the QM9 dataset consisting 133,015 small organic molecules (Wu et al. 2018) as well as the test set of the GuacaMol dataset which includes 238,706 molecules (Brown et al. 2019) for our experiments in Section 3.3.

3.1 Generative performance and distribution learning

We use standard benchmarks to evaluate the quality of MAGNet’s generation process. To complement this evaluation on the sampling quality, we further analyse to what degree different models sample uncommon shapes and, specifically for MAGNet, the quality of allocated atom and bond types.

MAGNet is the best AAO model on standard benchmarks The GuacaMol benchmark provides a framework for assessing the ability of a generative model to sample in accordance with the distribution of a molecular dataset (Brown et al. 2019). Next to the uniqueness of sampled molecules, and the novelty of the generated molecules, the GuacaMol benchmark also computes distributional

Table 1: GuacaMol and MOSES Benchmark. We report mean and standard deviation using 5 random seeds and highlight the best overall as well as **the best within each category**.

		All-At-Once		Sequential		
		PS-VAE	MAGNet	HierVAE	JTVAE	MoLeR
GM	(↓) FCD	3.63 ± 0.02	1.61 ± 0.02	2.57 ± 0.23	1.34 ± 0.00	1.24 ± 0.01
	(↑) KL	0.83 ± 0.00	0.92 ± 0.00	0.92 ± 0.00	0.94 ± 0.00	0.98 ± 0.00
MOSES	(↑) IntDiv	0.89 ± 0.00	0.88 ± 0.00	0.86 ± 0.00	0.86 ± 0.00	0.87 ± 0.00
	(↑) IntDiv2	0.88 ± 0.00	0.87 ± 0.00	0.85 ± 0.00	0.86 ± 0.00	0.86 ± 0.00
	(↓) logP	0.31 ± 0.02	0.38 ± 0.06	0.27 ± 0.07	0.27 ± 0.04	0.11 ± 0.03
	(↓) SA	1.19 ± 0.02	0.24 ± 0.03	0.15 ± 0.08	0.33 ± 0.01	0.06 ± 0.01
	(↓) QED	0.05 ± 0.00	0.01 ± 0.00	0.03 ± 0.01	0.01 ± 0.00	0.02 ± 0.00

distances to the reference. For this, the KL-divergence is used as a direct comparison of the reference and sampled distributions, while the Fréchet distance is computed via the ChemNet model, therefore, providing an indirect assessment (FCD). In addition to GuacaMol, the MOSES benchmark (Polykovskiy et al. 2020) computes measures for the internal diversity of the generated distribution (IntDiv & IntDiv2) as well chemical properties such as the synthetic accessibility (SA), the octanol-water partition coefficient (logP) or the viability for drugs (QED). For these properties, the 1-Wasserstein distance to the reference distribution is computed.

To run the benchmarks, we sample latent codes from the prior distribution, $z \sim P$, 10^4 in total, and decode them for all considered models. Our results for both benchmarks on the ZINC dataset are depicted in Table 1. While MoLeR sets the state of the art on both FCD and KL, MAGNet performs competitively overall, being better than HierVAE and clearly outperforming PS-VAE. Since MAGNet is AAO itself, this is already a very promising result, supporting the proposed factorisation in Section 2.1 while also challenging the common perception that methods for molecule generation must rely on motif vocabularies.

MAGNet samples uncommon shapes more accurately While the FCD is one of the most important metrics for molecular distribution learning, we find that it fails to provide insights about the specific molecules that are generated. We thus provide a more detailed comparison of MAGNet and existing models that rely on a combination of motifs and single atoms. If these models are able to represent any scaffold that is too rare to be included in the vocabulary, they should be able to reflect the reference distribution of shapes. Fig. 3a shows that this is *not* the case in practice. For this evaluation, we decompose the sampled molecules from the benchmark evaluation into their shapes. We then measure the models’ over- and undersampling behaviour based on the ratio r_{S_i} :

$$r_{S_i} = \frac{c_s(S_i)}{\sum_k c_s(S_k)} \times \frac{\sum_k c_t(S_k)}{c_t(S_i)}, \quad (1)$$

where c_t and c_s refer to the count function applied to the training set and sampled sets, respectively. On common shapes, i.e. those that occur in more than 5% of the molecules, all evaluated models are able to match the ratio of the ZINC distribution. On the tail of the shape distribution, however, both MoLeR and PS-VAE fail: while PS-VAE heavily oversamples both ring-like structures and chain-

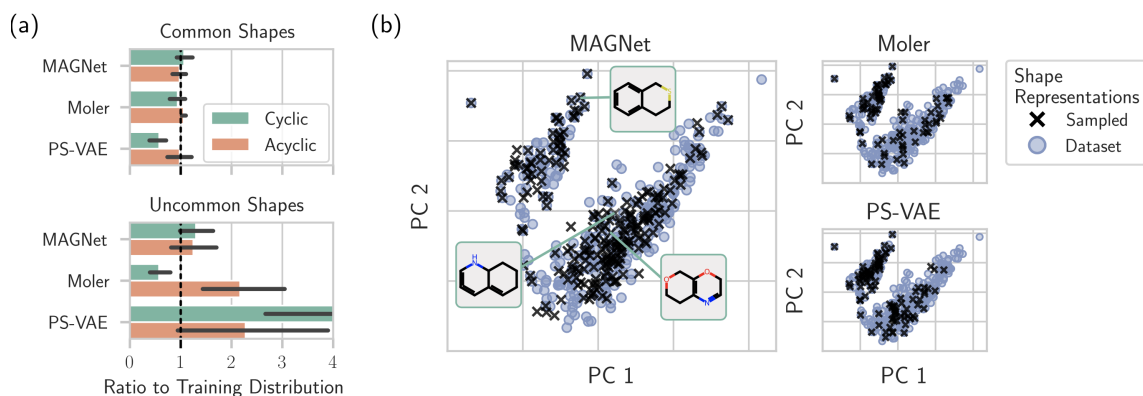


Figure 3: (a) Comparison of sampled shapes to shape occurrences in the training distribution. A ratio of 1 is optimal. (b) Qualitative example of the problem that motif-based approaches face: only MAGNet is able to adequately capture the dataset distribution.

like structures, MoLer oversamples chain-like structures and undersamples ring-like structures. MAGNet is able to closely match the distribution across categories and specifically in its tails, that is, MAGNet samples rare shapes reliably.

MAGNet’s shape representations are superior to fixed motifs The larger a given shape, the more the combinatorial aspect starts to dominate: with a size-limited vocabulary, it is challenging to reflect the diversity of a shape’s realisations during decoding. This is reflected in Fig. 3b, which provides a qualitative view on shape representations. We extract shape representations of a given shape from the molecules sampled in Table 1 and plot the two principal components of their fingerprints. Only for this shape, there are 339 representations in ZINC. Both PS-VAE as well as MoLeR are able to only barely cover the distribution. For this shape, 3.6 % of PS-VAE’s shape representations and 90% of MoLeR’s shape representations can be found in the respective vocabularies, indicating the reason behind its lacking ability to cover all shape representations sufficiently. We provide further analysis on this common observation in Appendices D and G. MAGNet, on the other hand, covers all parts of the distribution, even outliers. The results in Fig. 3b can be quantified by linear MMD, where MAGNet achieves a score of 0.17, while MoLeR and PS-VAE attain only scores of 1.72 and 3.35, respectively.

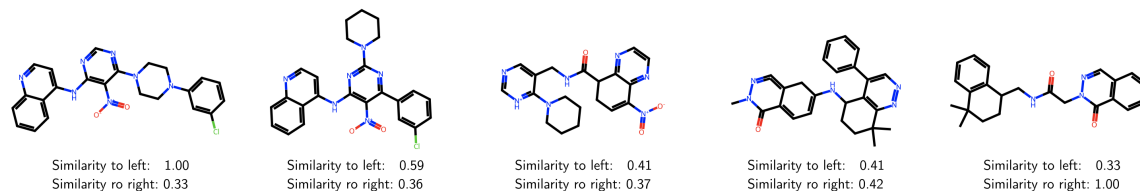


Figure 4: Interpolation between the latent space representations of two molecules with similar shape multiset \mathcal{S} and the similarity to both across decoded molecules.

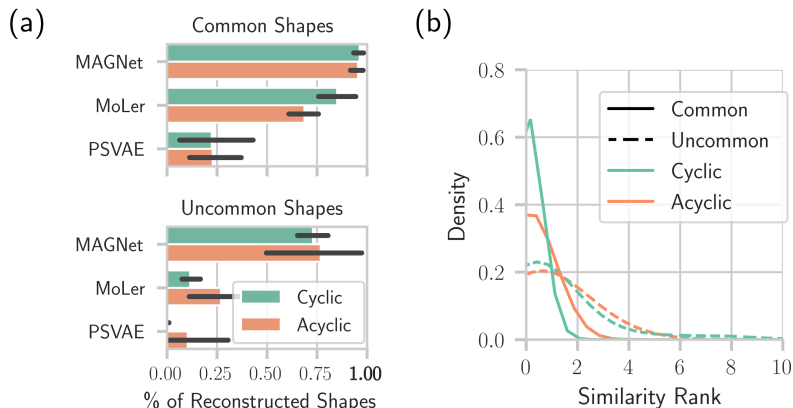


Figure 5: (a) Percentage of reconstructed shapes. MAGNet substantially improves in reconstructing both common and—more importantly—uncommon shapes. (b) Similarity rank for the reconstruction of shape representations.

Latent space interpolation To analyse both how MAGNet’s global context influences the decoding and how a shape’s location determines its representation M , we interpolate between the latent representation of two molecules, see Fig. 4. MAGNet’s latent space reflects a notion of similarity, as the transition in Tanimoto similarity changes smoothly. Once again, we can observe the universality of a shape vocabulary: while the shape multiset across decoded molecules is similar, they vary significantly in both their shape connectivity A and shape representations M . More examples for interpolation are shown in Appendix E.

3.2 MAGNet is more expressive

Having established the high quality of molecules generated by MAGNet, we want to evaluate its expressive power. While exact reconstruction is not suited to measure generative performance, it is a useful tool in this context: For the decoder, there should not be any stronger signal for generating a certain molecule than the latent code of exactly that molecule. Being able to *reliably* decode a large variety of molecular scaffolds is especially important for downstream tasks such a molecule optimisation.

Shape reconstruction We investigate how well different models can reconstruct the shape set \mathcal{S} for a given input molecule. For this analysis, we can disregard the shape connectivity A and representations M as we are only analysing $\mathbb{P}(\mathcal{S} | z)$. Fig. 5a depicts our results; we observe that MAGNet outperforms both MoLer and PS-VAE. Interestingly, this experiment highlights a shortcoming of purely motif-based vocabulary: while a 6-atom ring is considered a common shape, motif-based approaches can only reliably reconstruct such rings in the input if their atom/bond allocation is present in the vocabulary. Otherwise, these approaches appear to struggle to build such structures from single atoms. By contrast, MAGNet reliably decodes shapes.

Table 2: (left) Zero-shot generalisation performance on other datasets. (right) Sampling from QM9 via GMM fit. We report mean and standard deviation and highlight **the best overall**.

		PS-VAE	MAGNet	MoLeR			PSVAE	MAGNet	MoLeR
QM9	(↑) Tani.	0.11 ± 0.00	0.36 ± 0.01	0.29 ± 0.01	(↓) FCD	2.93 ± 0.03	2.44 ± 0.16	3.14 ± 0.09	
	(↑) Rec.	0.00 ± 0.00	0.10 ± 0.00	0.06 ± 0.00	(↑) KL	0.77 ± 0.00	0.82 ± 0.01	0.77 ± 0.00	
	(↑) KL	0.80 ± 0.00	0.92 ± 0.00	0.89 ± 0.01	(↑) Uni.	0.64 ± 0.02	0.82 ± 0.02	0.80 ± 0.04	
	(↓) FCD	2.47 ± 0.03	1.35 ± 0.00	1.98 ± 0.10					
GM	(↑) Tani.	0.34 ± 0.00	0.55 ± 0.00	0.47 ± 0.00	(↑) IntDiv	0.92 ± 0.00	0.92 ± 0.00	0.90 ± 0.00	
	(↑) Rec.	0.00 ± 0.00	0.07 ± 0.00	0.04 ± 0.00	(↑) IntDiv2	0.88 ± 0.00	0.90 ± 0.00	0.89 ± 0.00	
	(↑) KL	0.81 ± 0.01	0.93 ± 0.01	0.98 ± 0.00					
	(↓) FCD	5.56 ± 0.10	1.40 ± 0.01	1.33 ± 0.01					

Allocation of atom and bonds to shapes Building on the sampling analysis in Fig. 3a, we quantify the process of turning an abstract shape into a chemically valid substructure in Fig. 5b. For each shape in the ZINC dataset, we compute the similarities between the set of all decoded and ground truth allocations. Given a ground truth assignment and a successful shape decoding, we measure how the decoded allocation ranks compared to all known allocations. In the majority of cases, MAGNet achieves rank 0 or 1 in the shape allocation, with uncommon rings being the most challenging to decode.

3.3 Flexibility

To further highlight the flexibility of MAGNet’s shape abstraction and investigate the constraints of motif vocabularies, we examine its transferability to unseen datasets with distinct molecular distributions. Table 2 shows results for zero-shot generalization for the reconstruction task on 10^4 molecules from a given dataset. We then measure the pairwise Tanimoto similarity between input and decoded molecule, the number of exact matches as well as the FCD between reference distribution and decoded molecules. For experiment specification as well as an in-depth of MAGNet’s shape vocabulary for the unseen datasets we refer to Appendix F. Importantly, we use the vocabulary extracted from ZINC and do not finetune any model on the unseen datasets.

MoLeR and MAGNet perform similarly on the GuacaMol dataset, but MoLeR’s performance is lacking on the supposedly easier-to-learn dataset QM9. We can investigate this further by fitting a Gaussian Mixture Model (GMM) on the embeddings of each model for the given molecules in QM9. By sampling from this GMM, the models can sample from a dataset distribution that it was not trained on. Again, MAGNet outperforms all baselines significantly in all measured benchmark metrics. Importantly, MAGNet achieves a low FCD while retaining the highest Uniqueness and Internal Diversity measured. Despite all datasets containing drug-like molecules, MoLeR cannot capture the distribution of QM9, neither with its vocabulary nor through single atoms. Overall, these results highlight MAGNet’s ability to learn not only the underlying distribution of its training dataset, but to generalize to the larger space of drug-like molecules.

Limitations While we believe that the global context of MAGNet has many benefits useful for drug discovery, our method can suffer from error propagation. That is, if a generated shape graph

does not match the underlying distribution, it can be difficult for MAGNet to find sensible shape allocations or joins. At the current stage, we consider this the main reason why MAGNet can not achieve state-of-the-art results in terms of generative performance as measured by the FCD. Yet, we are confident that is an issue that can be solved through an adjusted training scheme or a more sophisticated sampling procedure.

4 Related Work

The literature on molecule generation can be classified by how a molecule is represented (Yu and Gao 2022; Yang et al. 2022; Zhu et al. 2022). 1D molecule generation treats inputs as SMILES, SMARTS or SELFIES strings, 2D molecule generation treats it as a graph with nodes and edges and 3D generation takes into account each atoms coordinates in a three-dimensional space. While 1D representations struggle with lacking invariances, they have recently gained attention with the rise of language models (Flam-Shepherd, Zhu, and Aspuru-Guzik 2022; Fang et al. 2023; Adilov 2021; Grisoni 2023). Within 2D generation models can be further classified into **all-at-once models** (Simonovsky and Komodakis 2018; Ma, Chen, and Xiao 2018; Liu et al. 2021; De Cao and Kipf 2018; Zang and Wang 2020; Bresson and Laurent 2019; Flam-Shepherd, Wu, and Aspuru-Guzik 2020; Samanta et al. 2019; Kong et al. 2022) and **sequential models** (Khemchandani et al. 2020; Shi et al. 2020; Popova et al. 2019; Mercado et al. 2021; Luo, Yan, and Ji 2021; Liu et al. 2018; Li et al. 2018; Assouel et al. 2018; Ahn et al. 2021; You et al. 2019; Yang et al. 2021; Lim et al. 2020; Kajino 2019; Jin, Barzilay, and Jaakkola 2020; Bengio et al. 2021). Compared to MAGNet, there are two recent works that are close in spirit. (Shirzad et al. 2022) focus on molecule generation through the lens of tree decomposition, where nodes in the tree represent clusters of nodes. (Ahn et al. 2021) generate subgraphs on-the-fly by building up subgraphs atom-by-atom.

5 Conclusion

We present MAGNet, a generative model for molecules that relies on a global context for its entire decoding procedure and disentangles structure from features while doing so. The proposed abstraction to shapes is a general concept and holds the potential to be applied for graph generation outside of the molecular world. Further, while we argue that a global context is important for shape representations, modifications of it can be promising also for sequential models. The flexibility and expressiveness of our model directly translate to good transfer results, suggesting MAGNet as a great candidate to be used in various downstream and application tasks, such as perturbation prediction or multi-resolution conditioning.

Acknowledgements

JS and LH are thankful for valuable feedback from David Lüdke, John Rachwan, Tobias Schmidt, Simon Geisler, and the DAML group and Theis Lab. LH is supported by the Helmholtz Association under the joint research school "Munich School for Data Science - MUDS".

References

- Adilov, Sanjar (2021). *Neural Language Modeling for Molecule Generation*. DOI: [10.26434/chemrxiv.14700831.v1](https://doi.org/10.26434/chemrxiv.14700831.v1).
- Ahn, Sungsoo et al. (2021). "Spanning tree-based graph generation for molecules". In: *International Conference on Learning Representations*.
- Assouel, Rim et al. (2018). *DEFactor: Differentiable Edge Factorization-based Probabilistic Graph Generation*. Tech. rep. arXiv. DOI: [10.48550/arXiv.1811.09766](https://doi.org/10.48550/arXiv.1811.09766).
- Bengio, Emmanuel et al. (2021). *Flow Network based Generative Models for Non-Iterative Diverse Candidate Generation*. Tech. rep. Neural Information Processing Systems.
- Bian, Yuemin and Xiang-Qun Xie (2021). "Generative chemistry: drug discovery with deep learning generative models". In: *Journal of Molecular Modeling*. ISSN: 0948-5023. DOI: [10.1007/s00894-021-04674-8](https://doi.org/10.1007/s00894-021-04674-8).
- Bresson, Xavier and Thomas Laurent (2019). *A Two Step Graph Convolutional Decoder for Molecule Generation*. Tech. rep. Machine Learning and the Physical Sciences Workshop. DOI: [10.48550/arXiv.1906.03412](https://doi.org/10.48550/arXiv.1906.03412).
- Brown, Nathan et al. (2019). "GuacaMol: Benchmarking Models for de Novo Molecular Design". In: *Journal of Chemical Information and Modeling*. ISSN: 1549-9596, 1549-960X. DOI: [10.1021/acs.jcim.8b00839](https://doi.org/10.1021/acs.jcim.8b00839).
- Butler, Keith T. et al. (2018). "Machine learning for molecular and materials science". In: *Nature*. ISSN: 1476-4687. DOI: [10.1038/s41586-018-0337-2](https://doi.org/10.1038/s41586-018-0337-2).
- Choudhary, Kamal et al. (2022). "Recent advances and applications of deep learning methods in materials science". In: *npj Computational Materials*. ISSN: 2057-3960. DOI: [10.1038/s41524-022-00734-6](https://doi.org/10.1038/s41524-022-00734-6).
- De Cao, Nicola and Thomas Kipf (2018). *MolGAN: An implicit generative model for small molecular graphs*. Tech. rep. arXiv. DOI: [10.48550/arXiv.1805.11973](https://doi.org/10.48550/arXiv.1805.11973).
- Du, Yuanqi et al. (2022). *MolGenSurvey: A Systematic Survey in Machine Learning Models for Molecule Design*. Tech. rep. arXiv. DOI: [10.48550/arXiv.2203.14500](https://doi.org/10.48550/arXiv.2203.14500).
- Fang, Yin et al. (2023). *Molecular Language Model as Multi-task Generator*. DOI: [10.48550/arXiv.2301.11259](https://doi.org/10.48550/arXiv.2301.11259).
- Flam-Shepherd, Daniel, Tony Wu, and Alan Aspuru-Guzik (2020). *Graph Deconvolutional Generation*. Tech. rep. arXiv. DOI: [10.48550/arXiv.2002.07087](https://doi.org/10.48550/arXiv.2002.07087).
- Flam-Shepherd, Daniel, Kevin Zhu, and Alán Aspuru-Guzik (2022). "Language models can learn complex molecular distributions". In: *Nature Communications*. ISSN: 2041-1723. DOI: [10.1038/s41467-022-30839-x](https://doi.org/10.1038/s41467-022-30839-x).
- Grisoni, Francesca (2023). "Chemical language models for de novo drug design: Challenges and opportunities". In: *Current Opinion in Structural Biology*. ISSN: 0959-440X. DOI: [10.1016/j.sbi.2023.102527](https://doi.org/10.1016/j.sbi.2023.102527).
- Hetzel, Leon et al. (2022). "Predicting Cellular Responses to Novel Drug Perturbations at a Single-Cell Resolution". In: *Advances in Neural Information Processing Systems*.
- Hoffman, Samuel C. et al. (2022). "Optimizing molecules using efficient queries from property evaluations". In: *Nature Machine Intelligence*. ISSN: 2522-5839. DOI: [10.1038/s42256-021-00422-y](https://doi.org/10.1038/s42256-021-00422-y).

- Irwin, John J. et al. (2020). "ZINC20—A Free Ultralarge-Scale Chemical Database for Ligand Discovery". In: *Journal of Chemical Information and Modeling*. ISSN: 1549-9596. DOI: [10.1021/acs.jcim.0c00675](https://doi.org/10.1021/acs.jcim.0c00675).
- Jin, Wengong, Regina Barzilay, and Tommi Jaakkola (2018). *Junction Tree Variational Autoencoder for Molecular Graph Generation*. Tech. rep. International Conference on Machine Learning.
- (2020). *Hierarchical Generation of Molecular Graphs using Structural Motifs*. Tech. rep. International Conference on Machine Learning.
- Kajino, Hiroshi (2019). "Molecular Hypergraph Grammar with Its Application to Molecular Optimization". In: *Proceedings of the 36th International Conference on Machine Learning*. PMLR.
- Khemchandani, Yash et al. (2020). "DeepGraphMolGen, a multi-objective, computational strategy for generating molecules with desirable properties: a graph convolution and reinforcement learning approach". In: *Journal of cheminformatics*.
- Kingma, Durk P, Tim Salimans, and Max Welling (2015). "Variational Dropout and the Local Reparameterization Trick". In: *Advances in Neural Information Processing Systems*. Curran Associates, Inc.
- Kong, Xiangzhe et al. (2022). *Molecule Generation by Principal Subgraph Mining and Assembling*.
- Kusner, Matt J., Brooks Paige, and José Miguel Hernández-Lobato (2017). *Grammar Variational Autoencoder*. Tech. rep. arXiv. DOI: [10.48550/arXiv.1703.01925](https://doi.org/10.48550/arXiv.1703.01925).
- Landrum, G. (2010). *RDKit*.
- Li, Yujia et al. (2018). *Learning Deep Generative Models of Graphs*. Tech. rep. arXiv. DOI: [10.48550/arXiv.1803.03324](https://doi.org/10.48550/arXiv.1803.03324).
- Lim, Jaechang et al. (2020). "Scaffold based molecular design using graph generative model". In: *Chemical Science*. ISSN: 2041-6520, 2041-6539. DOI: [10.1039/C9SC04503A](https://doi.org/10.1039/C9SC04503A).
- Liu, Meng et al. (2021). *GraphEBM: Molecular Graph Generation with Energy-Based Models*. Tech. rep. arXiv.
- Liu, Qi et al. (2018). *Constrained Graph Variational Autoencoders for Molecule Design*. Tech. rep. Advances in Neural Information Processing Systems.
- Luo, Youzhi, Keqiang Yan, and Shuiwang Ji (2021). *GraphDF: A Discrete Flow Model for Molecular Graph Generation*. Tech. rep. International Conference on Machine Learning.
- Ma, Tengfei, Jie Chen, and Cao Xiao (2018). *Constrained Generation of Semantically Valid Graphs via Regularizing Variational Autoencoders*. Tech. rep. Advances in Neural Information Processing Systems.
- Maziarz, Krzysztof et al. (2022). *Learning to Extend Molecular Scaffolds with Structural Motifs*. Tech. rep. arXiv.
- Mercado, Rocío et al. (2021). "Graph Networks for Molecular Design". In: *Machine Learning: Science and Technology*.
- Moret, Michael et al. (2023). "Leveraging molecular structure and bioactivity with chemical language models for de novo drug design". In: *Nature Communications*. ISSN: 2041-1723. DOI: [10.1038/s41467-022-35692-6](https://doi.org/10.1038/s41467-022-35692-6).
- Polykovskiy, Daniil et al. (2020). *Molecular Sets (MOSES): A Benchmarking Platform for Molecular Generation Models*. DOI: [10.48550/arXiv.1811.12823](https://doi.org/10.48550/arXiv.1811.12823).
- Popova, Mariya et al. (2019). *MolecularRNN: Generating realistic molecular graphs with optimized properties*. Tech. rep. arXiv. DOI: [10.48550/arXiv.1905.13372](https://doi.org/10.48550/arXiv.1905.13372).
- Samanta, Bidisha et al. (2019). *NeVAE: A Deep Generative Model for Molecular Graphs*. DOI: [10.48550/arXiv.1802.05283](https://doi.org/10.48550/arXiv.1802.05283).

- Shi, Chence et al. (2020). *GraphAF: a Flow-based Autoregressive Model for Molecular Graph Generation*. Tech. rep. arXiv. DOI: [10.48550/arXiv.2001.09382](https://doi.org/10.48550/arXiv.2001.09382).
- Shi, Yunsheng et al. (2021). *Masked Label Prediction: Unified Message Passing Model for Semi-Supervised Classification*. DOI: [10.48550/arXiv.2009.03509](https://doi.org/10.48550/arXiv.2009.03509).
- Shirzad, Hamed et al. (2022). "TD-GEN: Graph Generation Using Tree Decomposition". In: *Proceedings of The 25th International Conference on Artificial Intelligence and Statistics*. PMLR.
- Simonovsky, Martin and Nikos Komodakis (2018). *GraphVAE: Towards Generation of Small Graphs Using Variational Autoencoders*. DOI: [10.48550/arXiv.1802.03480](https://doi.org/10.48550/arXiv.1802.03480).
- Sommer, Johanna et al. (2023). "The Power of Motifs as Inductive Bias for Learning Molecular Distributions". In: .
- Weininger, David et al. (1989). "SMILES. 2. Algorithm for generation of unique SMILES notation". In: *Journal of Chemical Information and Computer Sciences*. ISSN: 0095-2338, 1520-5142. DOI: [10.1021/ci00062a008](https://doi.org/10.1021/ci00062a008).
- Wu, Zhenqin et al. (2018). *MoleculeNet: A Benchmark for Molecular Machine Learning*. DOI: [10.48550/arXiv.1703.00564](https://doi.org/10.48550/arXiv.1703.00564).
- Yang, Nianzu et al. (2022). *Molecule Generation for Drug Design: a Graph Learning Perspective*. Tech. rep. arXiv.
- Yang, Soojung et al. (2021). "Hit and Lead Discovery with Explorative RL and Fragment-based Molecule Generation". In: *Advances in Neural Information Processing Systems*.
- You, Jiaxuan et al. (2019). *Graph Convolutional Policy Network for Goal-Directed Molecular Graph Generation*. Tech. rep. arXiv. DOI: [10.48550/arXiv.1806.02473](https://doi.org/10.48550/arXiv.1806.02473).
- Yu, Zhaoning and Hongyang Gao (2022). "Molecular Representation Learning via Heterogeneous Motif Graph Neural Networks". In: *Proceedings of the 39th International Conference on Machine Learning*. PMLR.
- Zang, Chengxi and Fei Wang (2020). "MoFlow: An Invertible Flow Model for Generating Molecular Graphs". In: *Proceedings of the 26th ACM SIGKDD International Conference on Knowledge Discovery & Data Mining*. DOI: [10.1145/3394486.3403104](https://doi.org/10.1145/3394486.3403104).
- Zhou, Zhenpeng et al. (2019). "Optimization of Molecules via Deep Reinforcement Learning". In: *Scientific Reports*. ISSN: 2045-2322. DOI: [10.1038/s41598-019-47148-x](https://doi.org/10.1038/s41598-019-47148-x).
- Zhu, Yanqiao et al. (2022). *A Survey on Deep Graph Generation: Methods and Applications*.

A MAGNet fragmentation scheme

The MAGNet factorisation described in Section 2.1 requires shapes to be connected by joint atoms and not bonds. Thus, in the following section, “fragmenting on an atom” means that the specified atom stands as the connection between two fragment, i.e. it is shared between them.

The MAGNet fragmentation scheme on the core molecule starts from the “Breaking Bridge Bonds” (BBB) fragmentation, initially proposed in (Jin, Barzilay, and Jaakkola 2020) and extended in (Maziarz et al. 2022). BBB fragments a molecule by breaking all acyclic bonds adjacent to cyclic structures. Since MAGNet acts on shared atoms rather than bonds to connect structures, we fragment on those atoms that are present both in cyclic and acyclic structures. We make two further modifications to this procedure. If any two cyclic structures share a single atom, we fragment them into two separate fragments. Additionally, we do not break apart cyclic structures that act as junctions. That is, if any atom in a cyclic structure is part of more than one acyclic fragment, it will be left intact and handled as a junction later on.

Once all cyclic structures are fragmented, we turn to the remaining fragments. Again, due to the constraint that any atom can only be shared between two fragments, we further fragment on those atoms whose neighbours have degree three or higher. Importantly, we only fragment on those atoms that fulfill this condition but, at the same time, are not part of a ring, as we avoid taking apart rings.

B MAGNet: Hyperparameters and Training

Training MAGNet for one epoch takes less than 1 h on a single ‘NVIDIA GeForce GTX 1080 Ti’. We trained MAGNet for 40 epochs in total and conducted a random hyperparameter sweep including the learning rate, beta annealing scheme, and the number of layers for the encoder and latent module. The MAGNet model reported in the main text has 6.9 M parameters and its configuration is depicted in Table 3. In its current version, MAGNet processes roughly 70 molecules per second during training and samples about 8 molecules per second during inference.

Table 3: Parameter configuration of the best MAGNet run.

	Parameter	Value		Parameter	Value	
Train	batch_size	64	Model	node_aggregation	sum	
	lr	2.49×10^{-4}		num_layers_latent	2	
	lr_sch_decay	0.99		num_layers_enc	2	
	epochs	40		num_layers_shape_enc	4	
	gradclip	3		num_layers_hgraph	3	
Model	latent_dim	250	loss_weights	joins	1	
	enc_atom_dim	25		leaves	1	
	enc_shapes_dim	25		motifs	1	
	enc_joins_dim	25		hypergraph	1	
	enc_leaves_dim	25		beta_annealing	max	1
	enc_global_dim	25	init		0.01	
	dim_config	atom_id_dim	25		step	0.0005
	atom_charge_dim	10	every		100	
	atom_multiplicity_dim	10	start		2000	
	shape_id_dim	35				
	shape_multiplicity_dim	10				
	motif_feat_dim	50				
	shape_rnn_hidden	256				
	shape_gnn_dim	128				
	motif_seq_pos_dim	15				
leaf_rnn_hidden	256					

C Details Encoder

We build the node features that are processed in MAGNet’s encoder from different attributes, see Table 3. We include the atom type (‘atom_id_dim’), its charge (‘atom_charge_dim’), as well as its multiplicity value (‘atom_multiplicity_dim’). We proceed accordingly for the shape level and include the shape id (‘shape_id_dim’), its multiplicity (‘shape_multiplicity_dim’), as well chemical features (‘motif_feat_dim’) computed through RDKit (Landrum 2010). Since the latter are not learned during training, the features are mapped to the specified dimensionality by a linear map.

After processing the resulting node features through the graph transformer (Shi et al. 2021) with ‘num_layers_enc’-many layers, they are aggregated in different ways and mapped to specified dimensions as defined by ‘enc_<>_dim’ for the atoms, shapes, joins, and leaves, respectively. On top, the shape embeddings are additionally processed with the same transformer architecture (‘num_layers_shape_enc’) to inform the embedding about the shape-level connectivity. We then concatenate the resulting graph-level embeddings and further combine them with global molecule features, again computed via RDKit and then mapped to the required dimension (‘enc_global_dim’), before mapping them to the latent space via the latent module which has ‘num_layers_latent’-many layers.

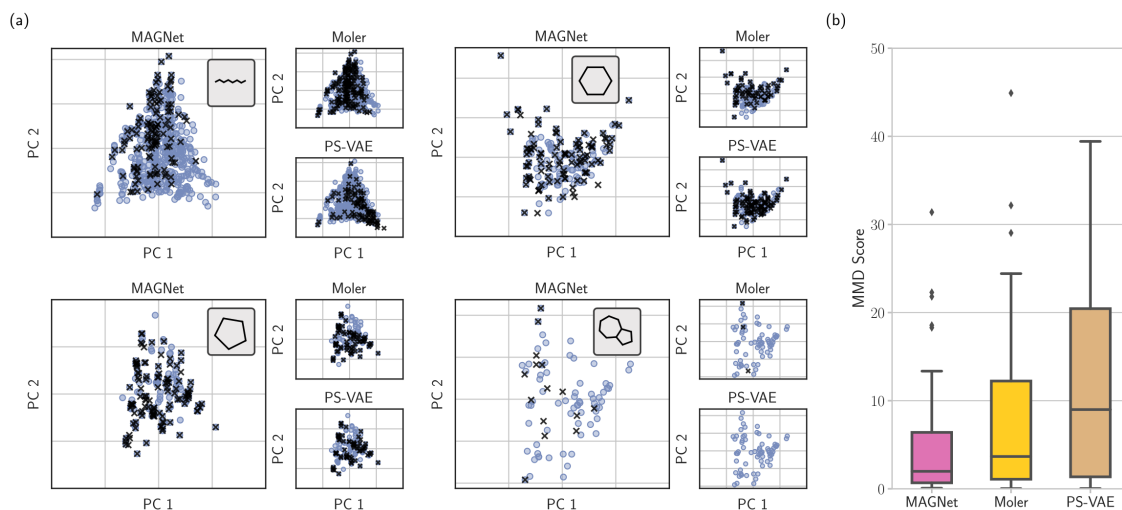


Figure 6: (a) Additional examples of shape allocations for four different shapes. MAGNet captures cyclic structures much better. For the chain, MoLeR seems to sample a greater variety within the sample set of 10^4 molecules. (b) Quantitative evaluation on alignment between sampled shape allocations and representations in the dataset. We report the MMD scores of all shapes that have at least eleven different shape representations.

D Additional Qualitative Shape Allocation Results

Supplementary to the results shown in Fig. 3, we provide more distribution plots in Fig. 6. Similarly, we compare the distribution of all shape allocations in the dataset to those sampled in a set of 10^4 molecules. We additionally provide MMD scores between sampled and ground truth shape allocations measured for all shapes with more than ten different allocations.

E Interpolation

Extending on Fig. 4, we provide more interpolation examples in Fig. 7. During interpolation, MAGNet stays faithful to the shapes present in the input molecules. The last row shows a failure case of MAGNet: it identifies a shape multiset that can not be fully connected to a molecule.

F Transferability of Shapes

We calculate the metrics presented in Table 2 (left) only for those molecules that can be represented via the shapes that were extracted from the ZINC dataset. For the QM9 dataset, MAGNet can represent roughly 72% of the molecules in the dataset. This is due to unseen shapes which make up around 14% out of the total set of 253,182 shapes. For GuacaMol, MAGNet can represent around 97% of the molecules in the dataset. Out of the 1,386,641 shapes in GuacaMol, only 0.6% are missing.

We consider a more flexible decomposition of shapes that translates even better across datasets important future work.

G Motif Vocabulary Experiment

Building on the performance of MoLeR in Section 3.1, Section 3.3 and Section 3.2, we investigate further to what extent MoLeR can decode structures that are not in the vocabulary. For this, we perform reconstruction and split the input molecule according to the BBB fragmentation and a vocabulary size 512. We measure for all motifs in the input that are *in the vocabulary* and *not in the vocabulary* whether this substructure can be found anywhere in the decoded molecule. The results in Fig. 9 show that the considered methods, here MoLeR, cannot reliably decode unknown motifs. In addition, cyclic shapes seem to be harder to decode than acyclic ones.

The consequences of this observation are discussed in Section 3.3, more specifically the Table 2 (left) on QM9, where the motif vocabulary does not represent many of the molecules’ substructures anymore. We provide qualitative examples of this in Fig. 8, where the model fails on comparably easy and small molecules from QM9 due to the fact that its motifs are not present in the vocabulary.

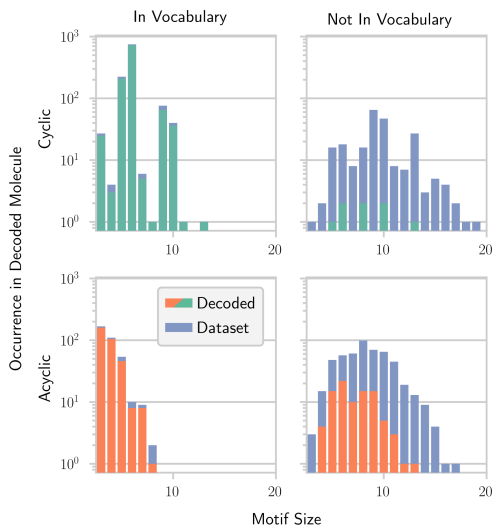


Figure 9: According to MoLeR’s fragmentation and vocabulary, we measure how many motifs are decoded anywhere in the output molecule during reconstruction. MoLeR can often not accurately decode substructures that are not part of its vocabulary.

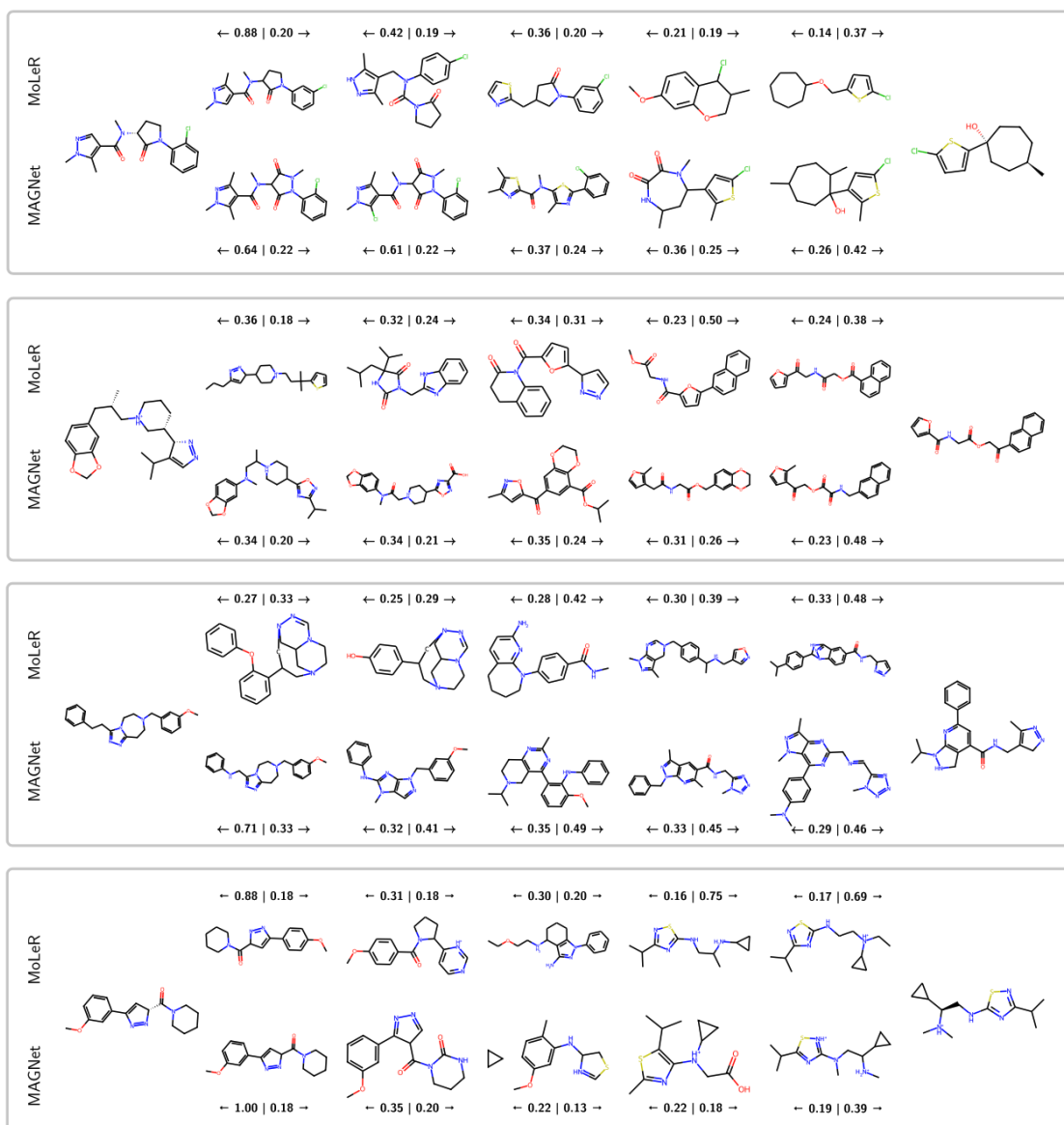


Figure 7: We provide four interpolation examples for MAGNet and MoLeR. The input molecules (left and right) are shared between the two models. We report the Tanimoto similarity as a rough estimate for the interpolation’s goodness.

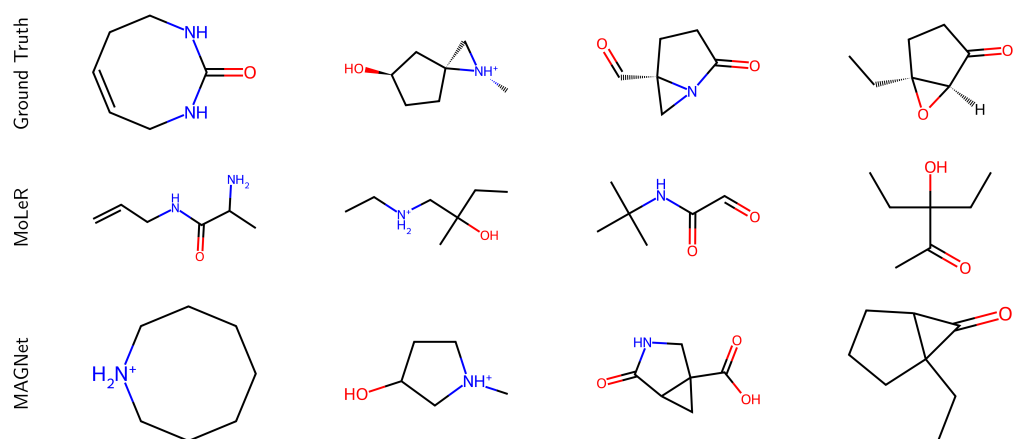


Figure 8: Qualitative example on how the reconstruction of molecules fails if a shape or its representation is not part of the motif vocabulary. Whilst MAGNet does not perform perfect reconstruction, its shape representation enable MAGNet to decode molecules more similar to the ground truth than MoLeR. All four molecules are part of the QM9 dataset.